

Collective Dynamics in Active Polar Polymer Assemblies

Hossein Vahid,¹ Jens-Uwe Sommer,^{1,2,*} and Abhinav Sharma^{3,1,†}

¹Leibniz-Institut für Polymerforschung Dresden, Bereich Theorie der Polymere, 01069 Dresden, Germany

²Technische Universität Dresden, Institut für Theoretische Physik, 01069 Dresden, Germany

³Faculty of Mathematics, Natural Sciences, and Materials Engineering: Institute of Physics, University of Augsburg, Universitätsstraße 1, 86159 Augsburg, Germany

(Dated: April 3, 2025)

Active polymers respond to spatial activity gradients by autonomously migrating, a behavior central to biological self-organization and the design of intelligent synthetic materials. Using Brownian dynamics simulations, we investigate how the structure and propulsion direction of tangentially driven active polymers (TDAPs) determine their collective response to activity gradients. We show that TDAP assemblies exhibit strikingly different behaviors based on their organization: inward-directed arms form compact bundles that accumulate in low-activity regions, whereas outward-directed arms assemble into asters that undergo directed motion toward high-activity regions. Remarkably, mixed structures—comprising both inward- and outward-directed arms—display enhanced accumulation in the high-activity regions due to cooperative effects. In addition, we show that two-arm polymers accumulate within a finite-width active slab embedded in a passive background, and as the slab narrows, the polymers reorient perpendicular to the slab boundaries to remain within the active regions. Our results establish a fundamental link between polymer geometry and emergent transport, providing key design principles for programmable active materials.

Introduction.— Polymers are essential to biological systems, forming structural and functional components across diverse cellular processes. Some self-organize into higher-order structures such as bundles, asters, and networks [1, 2]. These assemblies serve crucial functions: microtubule (MT) asters position centrosomes during mitosis [3–9], actin networks drive cellular migration [10–14], and filamentous bundles facilitate intracellular cargo transport [15]. Notably, many of these polymeric structures are active, driven far from equilibrium by molecular motors that exert forces along the polymer backbone [5, 16–21]. Inspired by biology, synthetic active systems have been designed to replicate and control such behaviors. Engineered MT asters [2, 22], actomyosin gels [5, 23], and colloidal self-assemblies [24–26] mimic biological functionality and respond to external signals such as light, magnetic fields, or chemical gradients.

Tangentially driven active polymers (TDAPs) are model systems, capturing key features of motor-driven filaments in biological systems [27–33]. Studies of homogeneous activity landscapes have revealed diverse emergent behaviors, including polar ordering, clustered aggregates, and vortex states [34, 35]. While these studies have primarily focused on high-density regimes where interactions dominate, the role of activity gradients—ubiquitous in biological and synthetic environments [5, 23, 36–41]—remains largely unexplored.

In this Letter, we investigate the behavior of TDAPs in spatially varying activity landscapes. We demonstrate that while isolated TDAPs accumulate in low-activity regions, structured assemblies such as asters exhibit a qualitatively different response. Strikingly, we find that asters undergo directed motion, with their trajectory determined by their geometry and propulsion mechanism. Finally, we explore how the width of an active slab em-

bedded in a passive medium controls polymer orientation. Our results provide fundamental insight into the self-organization of active polymers in non-uniform environments, with direct implications for both biological systems and the design of responsive synthetic materials.

The model.—We perform Brownian dynamics simulations to investigate semiflexible TDAPs and multi-arm TDAPs, see Fig. 1(a,b). Each TDAP monomer experiences a self-propulsion force $\mathbf{F}_a^i = f_a \mathbf{e}^i$, where f_a is the magnitude of the active force, and \mathbf{e}^i denotes the unit vector indicating the propulsion direction. The propulsion direction of each monomer (except for the polymer ends) at position \mathbf{r}^i is aligned with the local tangent vector of the polymer backbone, updated at each time step by $\mathbf{e}^i(t) = \mathbf{t}^i/|\mathbf{t}^i|$, where $\mathbf{t}^i = \mathbf{r}^{i+1} - \mathbf{r}^{i-1}$, and \mathbf{r}^{i-1} and

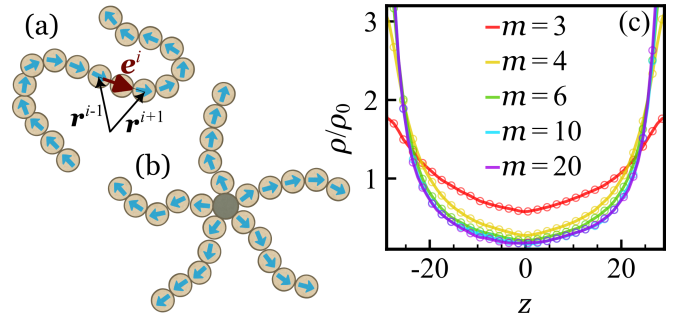


FIG. 1. Cartoon representation of (a) a TDAP and (b) an aster. Each active monomer is self-propelled in the direction of the local tangent to the backbone as indicated by the blue arrows. (c) Steady-state density of monomers along the z axis for varying degrees of polymerization, m , with $\rho_0 = 0.002$. Polymers are simple TDAPs as in (a), and the activity field is given by $f_a = 10(1 - |z|/30)$. TDAPs accumulate in the low-activity regions.

\mathbf{r}^{i+1} represent the positions of the adjacent monomers. For the first and last monomers of the chains, \mathbf{e}^i aligns with the bond connecting them to their nearest neighbor monomers.

The equation of motion of each monomer is described by $\gamma_t \dot{\mathbf{r}}^i = -\sum_j \nabla_{\mathbf{r}^i} U^{ij} + \mathbf{F}_a^i + \boldsymbol{\xi}^i(t)$, where γ_t is the translational friction coefficient of particle i , and U the potential energy. The stochastic noise $\boldsymbol{\xi}^i(t)$ is Gaussian, with zero mean $\langle \boldsymbol{\xi}^i(t) \rangle = 0$ and autocorrelation function $\langle \xi_\alpha^i(t) \cdot \xi_\beta^j(t') \rangle = 2\gamma_t^{-1} k_B T \delta^{ij} \delta_{\alpha\beta} \delta(t-t')$, where k_B is the Boltzmann constant, T the temperature, and $\alpha, \beta \in \{x, y, z\}$. Interparticle interactions are modeled using the Weeks-Chandler-Andersen (WCA) potential [42], $U_{\text{WCA}}^{ij}(r) = 4\epsilon [(\frac{\sigma^{ij}}{r^{ij}})^{12} - (\frac{\sigma^{ij}}{r^{ij}})^6 + \frac{1}{4}] \Theta(r_c^{ij} - r^{ij})$, where r^{ij} is the distance between particles i and j , and $\sigma^{ij} = 0.5(\sigma^i + \sigma^j)$ is their effective interaction diameter, with σ^i being the diameter of particle i . Here, ϵ is the depth of the potential well, Θ is the Heaviside step function, and the cutoff radius is set to $r_c^{ij} = 2^{1/6} \sigma^{ij}$.

In addition to WCA interactions, the bonded monomers are connected using the finite extensible nonlinear elastic (FENE) potential [43], defined as $U_F(r) = -\frac{1}{2} k_F R_0^2 \ln[1 - (\frac{r^{ij}}{R_0})^2] \Theta(R_0 - r^{ij})$, where k_F represents the elastic coefficient and R_0 is the maximum bond length. The chain conformation is controlled by the bending potential $U_b = k_b [1 - \cos(\theta - \theta_0)]$, where k_b is the bending modulus, θ the angle between consecutive bonds, and θ_0 the rest angle.

We set $\sigma = 1$, $\epsilon = k_B T = 1$, and $\tau = \sigma^2 \gamma_t / (3k_B T)$, with $\gamma_t = 3$, as the units of length, energy, and time, respectively. All other physical quantities are measured in terms of these fundamental units. All simulations are conducted using the LAMMPS [44, 45] package within a cubic simulation box of dimensions $60 \times 60 \times 60 \sigma^3$, ranging from -30 to 30 along each axis. Periodic boundary conditions are imposed in all directions. The activity field varies linearly along the z -axis according to $f_a = f_a^* (1 - |z|/30)$, where $f_a = f_a^*$ at the box center $z = 0$, and $f_a = 0$ at $|z| = 30$. The systems studied contain N monodisperse chains, each with m monomers. The bulk density is defined as $\rho_0 = Nm/60^3$. The time step is set to $5 \times 10^{-4} \tau$. Each simulation runs for 2×10^8 steps, and the last 1.5×10^8 steps are used for data analysis. Trajectories are recorded every 2000 step. Steady-state density profiles of monomers along the z -axis are calculated as $\rho(z) = \langle n(t) \rangle_t / (60^2 \Delta z)$, where $\langle n(t) \rangle_t$ is the time-averaged number of monomers within a slab of thickness $\Delta z = 0.6$ centered at position z . The simulation parameters are set to $\sigma^i = 1$, $k_F = 30$, $R_0 = 2\sigma^i$, $k_b = 30$, and $\theta_0 = 120^\circ$.

Results.—We first study individual TDAP chains. Fig. 1(c) shows these polymers tend to accumulate in the low-activity regions, regardless of the chain length. TDAP propulsion aligns with the polymer backbone, and thus following the motions of their head monomers,

TDAP chains preferentially orient and accumulate toward lower-activity regions. In contrast, active Brownian polymers (ABPOs) display length-dependent accumulation and migrate to the high-activity regions as the chain length m increases [46–48]; see Fig. S1 of the Supplementary Material (SM).

In many biological systems, active filaments are observed in assembled structures, such as bundles and asters [3, 4, 6–14]. Figure 2 shows that the directed motion and the overall conformation of two connected TDAPs are significantly influenced by their relative propulsion directions. We connect two TDAP arms, each consisting of m monomers, to a central passive core. We consider two distinct configurations: inward-directed (tangential propulsion from the arm tips toward the core, Fig. 2(a)) and outward-directed (from the core toward the arm tips, Fig. 2(b)). In the inward-directed case, the two arms tend to approach each other, which again leads to accumulation in lower-activity regions. Inward propulsion creates effective inward-directed stresses leading to arm folding at the core position that stabilizes their collective migration toward low activity. Notably, variations in m do not significantly influence this behavior.

For outward-directed propulsion, the two arms exhibit a tug-of-war dynamic [49]. The tug-of-war of motor proteins was also found to be highly cooperative and perform directed cargo transport [50]. Here, propulsion forces stretch the polymer, and the polymer migrates toward high-activity regions. This occurs because when one arm aligns toward regions of higher activity, it experiences a stronger active force, pulling the entire polymer toward that region. It is consistent with previous studies on rigid dimers of ABPs, where outward-propelling dimers generate a net force leading to accumulation in high-activity regions, whereas inward-propelling dimers migrate toward low-activity regions [51]. As arm length increases, monomers tend to accumulate in high-activity regions, but their spatial distribution becomes broader, and the peak density at the highest activity decreases. Since the

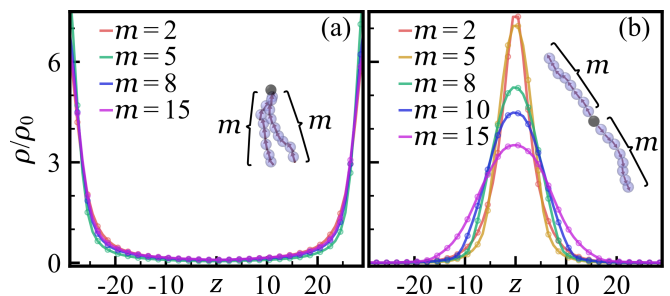


FIG. 2. Steady-state density of monomers along the z axis. Polymers have two symmetric TDAP arms, each containing m monomers, connected to a passive core. (a) TDAPs are directed toward the core and accumulate in the low-activity regions. (b) TDAPs are directed away from the core and migrate to high-activity regions.

polymer remains nearly stretched, not all monomers can occupy the same z position. While the core remains in the high-activity region (see Fig. S5 of SM), the extended arms reach lower-activity areas. Furthermore, our results show that as the polymer becomes more stretched (increasing θ_0) or stiffer (increasing k_b), the accumulation in the high-activity regions enhances (cf. Fig. S6 of SM).

We next examine how asymmetry in arm length affects the accumulation behavior of these assemblies. In biological systems, cross-linked actin and MT structures often exhibit asymmetric arm lengths [23]. As expected, increasing asymmetry eventually leads to accumulation in low-activity regions. Interestingly, at intermediate asymmetry, polymers accumulate in the intermediate activity regions due to the competition between arms (cf. Fig. S7 of SM).

Although the above results highlight the fundamental response of two-arm TDAPs to activity gradients, cytoskeletal networks and cellular assemblies often have more arms [52, 53]. In Fig. 3, findings for multi-arm polymers, each containing five monomers ($m = 5$) extending from a central passive core, are presented. We examine inward-directed propulsion (toward the central core, Fig. 3(a)) and outward-directed propulsion (away from the core, Fig. 3(b)). For inward-directed propulsion, the active arms tend to collapse close to each other, forming compact, bundle-like structures. These arms cooperatively move toward the low-activity region, and increasing the number of arms enhances accumulation in that region.

In contrast, outward-directed propulsion leads to open radial structures, resembling asters. These asters accumulate in the high-activity regions. The accumulation displays nonmonotonic behavior with respect to the number of arms. Maximum accumulation in the high-activity region is achieved for the two-arm structure, which decreases dramatically when a third arm is added. Here, the three-arm polymer faces competition among arms oriented toward different activity levels, reducing the net

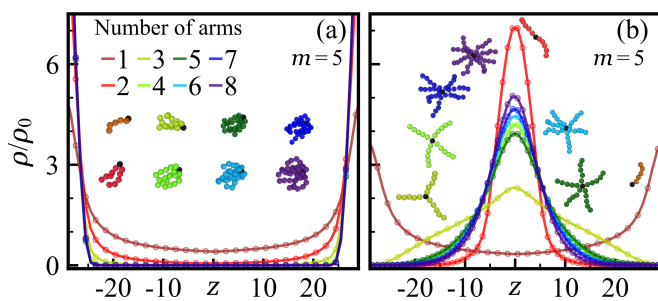


FIG. 3. Steady-state density of monomers along the z axis for polymers with varying numbers of arms. Each arm is an (a) inward- or (b) outward-directed TDAP with 5 monomers. The activity field is given by $f_a = 10(1 - |z|/30)$, and the bulk monomer density is set to $\rho_0 = 0.002$.

directional migration. Increasing the number of arms to four slightly improves accumulation relative to the three-arm structure. Further increases in arm number have minimal effects. These trends persist across different activity magnitudes (f_a^*) and bulk densities of TDAP (ρ_0) (see Fig. S9 the SM). At very high densities, accumulation extends to lower-activity regions because the high-activity regions become saturated.

Recent experiments demonstrated that inward- and outward-directed forces on MTs can be controlled using light-switchable motors [54] and by balancing motor forces with polymerization-driven expansion [23]. Additionally, layered asters can form in active MT-actin composites, where kinesin-driven MTs act as active arms, while actin filaments remain passive [55]. In Fig. 4(a), we examine polymers consisting of a varying number of passive arms (l) and $8-l$ outward-directed TDAP arms, each with $m = 5$ monomers. Increasing the number of passive arms from $l = 0$ to $l = 5$ progressively reduces aster accumulation in high-activity regions. At $l = 6$, where two arms are active, the polymer exhibits maximum accumulation in the high-activity region, consistent with our previous observation, Fig. 3(b), for two-arm polymers. At $l = 7$, polymers accumulate in low-activity regions. Panel (b) shows the behavior of polymers with mixed propulsion directions: l inward-directed TDAP arms (toward the core) and $8-l$ outward-directed TDAP arms (away from the core). Increasing the number of inward-directed arms from $l = 0$ to $l = 4$ reduces accumulation in the high-activity regions, with the minimal accumulation observed at $l = 5$, where three outward-directed arms compete strongly, resembling the reduced accumulation observed in three-arm asters (Fig. 3(b)). Surprisingly, at $l = 6$, with exactly two outward-directed TDAP arms, accumulation in high-activity regions is significantly enhanced. Here, the inward-directed arms cooperatively assist the two outward-directed arms, enabling strong collective migration toward high-activity regions. For $l > 6$, polymers migrate to low-activity regions.

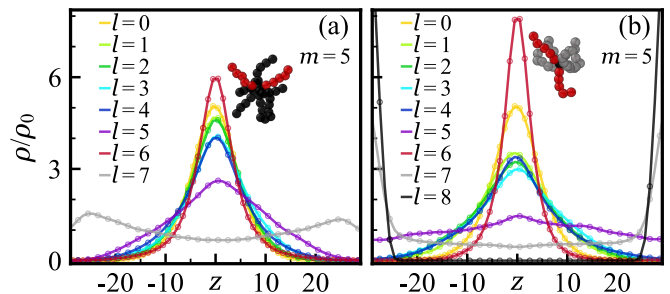


FIG. 4. Steady-state density of monomers along the z axis. Polymers have 8 arms, each with 5 monomers. (a) l arms are passive, and $8-l$ arms are outward-directed TDAPs. (b) l arms are inward-directed TDAPs, and $8-l$ arms are outward-directed TDAPs. The activity field is given by $f_a = 10(1 - |z|/30)$, and the bulk monomer density is set to $\rho_0 = 0.002$.

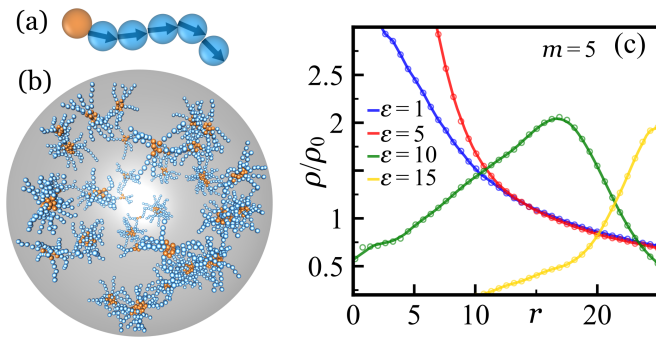


FIG. 5. (a) Schematic representation of a TDAP with $m = 5$ (blue) pulling a passive and attractive particle (orange). (b) A simulation snapshot of 400 TDAPs, each with $m = 5$ (blue) pulling a passive attractive particle (orange). The polymers are confined in a spherical shell with radius $r = 30$. The activity field is given by $f_a = 5r/30$, and $\epsilon = 15$. Polymers form asters and migrate toward the high-activity regions. (c) Steady-state density of monomers as a function of r for varying passive-passive attraction strength ϵ .

A characteristic of biopolymer assemblies is that they are transient structures that can disassemble into single filaments [9, 18, 19, 38, 56–61]. For example, actin filaments are temporarily cross-linked and reorganized through the activity of molecular motors such as myosin [62, 63] or buckling [64]. A recent experiment demonstrated that plus-end-directed KIF11 motors facilitate MT plus-end bundling and minus-end-directed HSET motors stabilize bundles at low concentrations but induce transitions to asters at higher concentrations [18]. Inspired by this, we perform simulations for TDAPs with 5 monomers, each pulling a passive and attractive particle connected to the tail (see Fig. 5(a)). The active force of the TDAPs is along their head. Polymers are confined within a spherical cell of radius $r = 30$ where the surface mimics the cortex as $f_a = 5r/30$. TDAP monomers interact via the WCA potential with other TDAP monomers and passive particles, whereas passive particles display attractive interactions among each other, which are described by the Lennard-Jones potential with an interaction well depth of ϵ (see Eq. (S2) of SM). The cortex is modeled as a spherical boundary at $r = 32.5$, interacting with all monomers and passive particles via a purely repulsive harmonic potential $E = 4(r - r_c)^2$ for $r < r_c$, where r is their distance from the cortex, and $r_c = 2.5\sigma$ defines the interaction cutoff distance.

Figure 5(c) shows that at weak attraction strengths ($\epsilon < 10$), active forces prevent stable assemblies leading to accumulation in the center of the sphere (low-activity). At $\epsilon \approx 10$, asters form and migrate towards higher activity regions, but before reaching the cortex at $r \approx 17$, the active forces dominate and disassemble the asters. For $\epsilon = 15$ the attraction is strong enough to maintain stable asters migrating to the cortex and accumulating there.

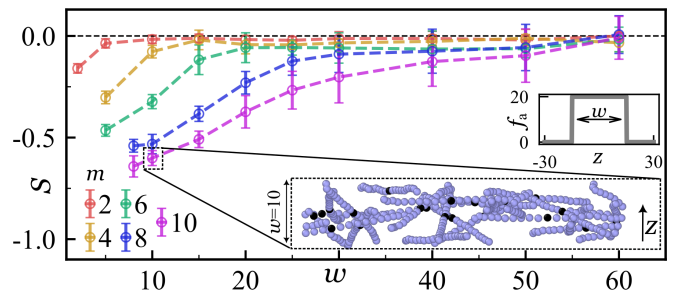


FIG. 6. Orientation order parameter S of two-arm polymers, each arm containing m monomers, in an active region of width w . Inset: activity field is given by $f_a(z) = 20[\Theta(z+w) - \Theta(z-w)]$. Snapshot shows two-arm outward-directed TDAPs, each arm with $m = 10$, in an active region of width $w = 10$.

It has been shown experimentally that spatially heterogeneous motor distributions guide filament alignment and accumulation [65, 66]. For example, MTs gliding over a fluid lipid membrane enriched with diffusible kinesin motors spontaneously form nematically ordered lanes within motor-dense regions [65]. To investigate similar mechanisms in a simplified geometry, we examine a system with an active slab of width w embedded in a passive background, defined by an activity field $f_a(z) = 20[\Theta(z+w) - \Theta(z-w)]$ in 3D; see inset of Fig. 6. Two-arm TDAPs, composed of outward-propelling arms of length m , are trapped in the active region, analogous to the findings presented in Fig. 2(b). To quantify their alignment, we calculate their orientation order parameter $S = 2\langle |\hat{u} \cdot \hat{z}| \rangle - 1$, where \hat{u} is the unit vector pointing from the monomer nearest the core on one arm to the corresponding monomer on the other arm, and \hat{z} is the unit vector along the z axis. Here, $S = 1$ indicates alignment along the z -axis, $S = -1$ perpendicular to it, and $S = 0$ random orientation. As the active slab narrows (lower w), polymers tend to align perpendicular to the z -axis, maximizing their presence within the active region.

To assess the robustness of our results, we systematically vary parameters such as polymer conformation, activity strength, concentration, and partial activation (see SM). Across these variations, our results remain consistent, demonstrating the generality of the observed behaviors.

In conclusion, assembling TDAPs into multi-arm structures switches their response to activity gradients. The propulsion direction of the individual arms determines where they migrate to and accumulate: one-end attached and inward-directed TDAPs form bundle-like structures accumulating in low-activity regions, while outward-directed TDAPs form aster-like structures migrating toward high-activity areas, with peaks observed for two-arm configurations. Mixed structures with two outward-directed and multiple inward-directed arms co-

operatively migrate toward high-activity regions, leading to enhanced accumulation in those regions. Our findings highlight the crucial interplay between polymer architecture, propulsion directionality, and collective organization in directing active matter. In particular, dynamic association of active chains through transient binding can lead to cyclic transport in activity gradients. Our findings could be experimentally tested using synthetic swimmers [67], synthetic chains of magnetic colloidal beads, where external fields control their assembly and motion, similar to magnetic colloidal asters [26]. Additionally, light patterns and light-controlled motor activation have also been used to generate and transport MT [5, 54] and actin [23, 37] assemblies such as asters, providing a potential method to explore the dynamics and stability of asters in inhomogeneous activity fields.

Acknowledgements.—A.S. acknowledges support by the Deutsche Forschungsgemeinschaft (DFG) within Project No. SH 1275/5-1. J.U.S. thanks the cluster of excellence “Physics of Life” at TU Dresden for its support.

* jens-uwe.sommer@tu-dresden.de

† abhinav.sharma@uni-a.de

- [1] Y. Vyborna, J.-C. Galas, and A. Estevez-Torres, *J. Am. Chem. Soc.* **143**, 20022 (2021).
- [2] Q. Xie, X. Chen, T. Wu, T. Wang, Y. Cao, S. Granick, Y. Li, and L. Jiang, *Nat. Commun.* **10**, 4954 (2019).
- [3] P. A. Nguyen, A. C. Groen, M. Loose, K. Ishihara, M. Wühr, C. M. Field, and T. J. Mitchison, *Science* **346**, 244 (2014).
- [4] K. Ishihara, P. A. Nguyen, A. C. Groen, C. M. Field, and T. J. Mitchison, *Proc. Natl. Acad. Sci.* **111**, 17715 (2014).
- [5] T. D. Ross, H. J. Lee, Z. Qu, R. A. Banks, R. Phillips, and M. Thomson, *Nature* **572**, 224 (2019).
- [6] Z. Feng, A. Caballe, A. Wainman, S. Johnson, A. F. Haensele, M. A. Cottee, P. T. Conduit, S. M. Lea, and J. W. Raff, *Cell* **169**, 1078 (2017).
- [7] J. B. Woodruff, B. F. Gomes, P. O. Widlund, J. Mahamid, A. Honigsmann, and A. A. Hyman, *Cell* **169**, 1066 (2017).
- [8] G. D. Gupta and L. Pelletier, *Curr. Biol.* **27**, R836 (2017).
- [9] S. R. Norris, S. Jung, P. Singh, C. E. Strothman, A. L. Erwin, M. D. Ohi, M. Zanic, and R. Ohi, *Nat. Commun.* **9**, 2659 (2018).
- [10] M. Soares e Silva, M. Depken, B. Stuhmann, M. Korsten, F. C. MacKintosh, and G. H. Koenderink, *Proc. Natl. Acad. Sci.* **108**, 9408 (2011).
- [11] F. Huber, D. Strehle, and J. Käs, *Soft Matter* **8**, 931 (2012).
- [12] M. Bovellan, Y. Romeo, M. Biro, A. Boden, P. Chugh, A. Yonis, M. Vaghela, M. Fritzsche, D. Moulding, R. Thorogate, *et al.*, *Curr. Biol.* **24**, 1628 (2014).
- [13] M. Fritzsche, D. Li, H. Colin-York, V. Chang, E. Moeendarbary, J. Felce, E. Sezgin, G. Charras, E. Betzig, and C. Eggeling, *Nat. Commun.* **8**, 14347 (2017).
- [14] H. Colin-York, D. Li, K. Korobchevskaya, V. T. Chang, E. Betzig, C. Eggeling, and M. Fritzsche, *Commun. Biol.* **2**, 93 (2019).
- [15] H. Tanimoto, A. Kimura, and N. Minc, *J. Cell Biol.* **212**, 777 (2016).
- [16] D. Chowdhury, *Physica A Stat. Mech. Appl.* **372**, 84 (2006).
- [17] J. Roostalu, J. Rickman, C. Thomas, F. Nédélec, and T. Surrey, *Cell* **175**, 796 (2018).
- [18] G. Henkin, W.-X. Chew, F. Nédélec, and T. Surrey, *Proc. Natl. Acad. Sci. U.S.A.* **119**, e2206398119 (2022).
- [19] B. Najma, W.-S. Wei, A. Baskaran, P. J. Foster, and G. Duclos, *Proc. Natl. Acad. Sci.* **121**, e2300174121 (2024).
- [20] R. Ananthakrishnan and A. Ehrlicher, *Int. J. Biol. Sci.* **3**, 303 (2007).
- [21] M. Bornens, *Science* **335**, 422 (2012).
- [22] T. Nitta, Y. Wang, Z. Du, K. Morishima, and Y. Hiratsuka, *Nat. Mater.* **20**, 1149 (2021).
- [23] M. Schuppler, F. C. Keber, M. Kröger, and A. R. Bausch, *Nat. Commun.* **7**, 13120 (2016).
- [24] M. N. Popescu, *Langmuir* **36**, 6861 (2020).
- [25] J. H. Bahng, B. Yeom, Y. Wang, S. O. Tung, J. D. Hoff, and N. Kotov, *Nature* **517**, 596 (2015).
- [26] A. Snezhko and I. S. Aranson, *Nat. Mater.* **10**, 698 (2011).
- [27] V. Schaller, C. Weber, C. Semmrich, E. Frey, and A. R. Bausch, *Nature* **467**, 73 (2010).
- [28] G. De Canio, E. Lauga, and R. E. Goldstein, *J. R. Soc. Interface* **14**, 20170491 (2017).
- [29] S. K. Anand and S. P. Singh, *Phys. Rev. E* **98**, 042501 (2018).
- [30] V. Bianco, E. Locatelli, and P. Malfaretti, *Phys. Rev. Lett.* **121**, 217802 (2018).
- [31] C. A. Philipps, G. Gompper, and R. G. Winkler, *J. Chem. Phys.* **157**, 10.1063/5.0120493 (2022).
- [32] J.-X. Li, S. Wu, L.-L. Hao, Q.-L. Lei, and Y.-Q. Ma, *Phys. Rev. Res.* **5**, 043064 (2023).
- [33] M. Fazelzadeh, E. Irani, Z. Mokhtari, and S. Jabbari-Farouji, *Phys. Rev. E* **108**, 024606 (2023).
- [34] C. Zhao, R. Yan, and N. Zhao, *J. Chem. Phys.* **161**, 10.1063/5.0225429 (2024).
- [35] R. E. Isele-Holder, J. Elgeti, and G. Gompper, *Soft matter* **11**, 7181 (2015).
- [36] C. J. Miller, P. K. LaFosse, S. B. Asokan, J. M. Haugh, J. E. Bear, and T. C. Elston, *Integr. Biol.* **11**, 280 (2019).
- [37] R. Zhang, S. A. Redford, P. V. Ruijgrok, N. Kumar, A. Mozaffari, S. Zemsky, A. R. Dinner, V. Vitelli, Z. Bryant, M. L. Gardel, *et al.*, *Nat. Mater.* **20**, 875 (2021).
- [38] C. Hentrich and T. Surrey, *J. Cell Biol.* **189**, 465 (2010).
- [39] S. Saha, R. Golestanian, and S. Ramaswamy, *Phys. Rev. E* **89**, 062316 (2014).
- [40] J. Palacci, S. Sacanna, A. P. Steinberg, D. J. Pine, and P. M. Chaikin, *Science* **339**, 936 (2013).
- [41] M. A. Ubertini, E. Locatelli, and A. Rosa, *ACS Macro Lett.* **13**, 1204 (2024).
- [42] J. D. Weeks, D. Chandler, and H. C. Andersen, *J. Chem. Phys.* **54**, 5237 (1971).
- [43] R. B. Bird, C. F. Curtiss, R. C. Armstrong, and O. Hassager, *Dynamics of polymeric liquids* (Wiley, New York, 1987).
- [44] S. Plimpton, *J. Comput. Phys.* **117**, 1 (1995).
- [45] A. P. Thompson, H. M. Aktulga, R. Berger, D. S.

- Bolintineanu, W. M. Brown, P. S. Crozier, P. I. Veld, A. Kohlmeyer, S. G. Moore, T. D. Nguyen, R. Shan, M. J. Stevens, J. Tranchida, C. Trott, and S. J. Plimpton, *Comp. Phys. Comm.* **271**, 108171 (2022).
- [46] H. D. Vuijk, H. Merlitz, M. Lang, A. Sharma, and J.-U. Sommer, *Phys. Rev. Lett.* **126**, 208102 (2021).
- [47] S. Ravichandir, B. Valecha, P. L. Muzzeddu, J.-U. Sommer, and A. Sharma, *Soft Matter* **21**, 1835 (2025).
- [48] P. L. Muzzeddu, A. Gambassi, J.-U. Sommer, and A. Sharma, *Phys. Rev. Lett.* **133**, 118102 (2024).
- [49] P. L. Muzzeddu, H. D. Vuijk, H. Löwen, J.-U. Sommer, and A. Sharma, *J. Chem. Phys.* **157**, 10.1063/5.0109817 (2022).
- [50] M. J. Müller, S. Klumpp, and R. Lipowsky, *Proc. Natl. Acad. Sci.* **105**, 4609 (2008).
- [51] H. D. Vuijk, S. Klempahn, H. Merlitz, J.-U. Sommer, and A. Sharma, *Phys. Rev. E* **106**, 014617 (2022).
- [52] C. A. Weber, R. Suzuki, V. Schaller, I. S. Aranson, A. R. Bausch, and E. Frey, *Proc. Natl. Acad. Sci.* **112**, 10703 (2015).
- [53] C. P. Brangwynne, G. H. Koenderink, F. C. MacKintosh, and D. A. Weitz, *J. Cell Biol.* **183**, 583 (2008).
- [54] L. M. Lemma, M. Varghese, T. D. Ross, M. Thomson, A. Baskaran, and Z. Dogic, *PNAS nexus* **2**, pgad130 (2023).
- [55] J. Berezney, B. L. Goode, S. Fraden, and Z. Dogic, *Proc. Natl. Acad. Sci.* **119**, e2115895119 (2022).
- [56] D. Gordon, A. Bernheim-Groswasser, C. Keasar, and O. Farago, *Phys. Biol.* **9**, 026005 (2012).
- [57] M. E. Tanenbaum, R. D. Vale, and R. J. McKenney, *Elife* **2**, e00943 (2013).
- [58] T. H. Tan, M. Malik-Garbi, E. Abu-Shah, J. Li, A. Sharma, F. C. MacKintosh, K. Keren, C. F. Schmidt, and N. Fakhri, *Sci. Adv.* **4**, eaar2847 (2018).
- [59] C. Utzschneider, B. Suresh, A. Sciortino, J. Gaillard, A. Schaeffer, S. Pattanayak, J.-F. Joanny, L. Blanchoin, and M. Théry, *Proc. Natl. Acad. Sci.* **121**, e2406985121 (2024).
- [60] A. Lamtyugina, D. S. Banerjee, Y. Qiu, and S. Vaikuntanathan, *bioRxiv*, 2024 (2024).
- [61] B. Lemma, N. P. Mitchell, R. Subramanian, D. J. Needleman, and Z. Dogic, *Phys. Rev. X* **12**, 031006 (2022).
- [62] J. Prost, F. Jülicher, and J.-F. Joanny, *Nat. Phys.* **11**, 111 (2015).
- [63] Y. H. Tee, T. Shemesh, V. Thiagarajan, R. F. Hariadi, K. L. Anderson, C. Page, N. Volkmann, D. Hanein, S. Sivaramakrishnan, M. M. Kozlov, *et al.*, *Nat. Cell Biol.* **17**, 445 (2015).
- [64] K. Matsuda, W. Jung, Y. Sato, T. Kobayashi, M. Yamagishi, T. Kim, and J. Yajima, *Cytoskeleton* **81**, 339 (2024).
- [65] F. L. Memarian, J. D. Lopes, F. J. Schwarzendahl, M. G. Athani, N. Sarpangala, A. Gopinathan, D. A. Beller, K. Dasbiswas, and L. S. Hirst, *Proc. Natl. Acad. Sci.* **118**, e2117107118 (2021).
- [66] L. Huber, R. Suzuki, T. Krüger, E. Frey, and A. Bausch, *Science* **361**, 255 (2018).
- [67] Y. Ji, X. Lin, Z. Wu, Y. Wu, W. Gao, and Q. He, *Angew. Chem.* **131**, 12328 (2019).

Supplemental Material for

Collective Dynamics in Active Polar Polymer Assemblies

This Supplemental Material presents additional results on active Brownian polymers, tangentially driven active polymers (TDAPs) with varying head activity, chain conformation, and arm asymmetry, as well as TDAPs pulling passive polymers and asters under different activity gradients and bulk densities.

ACTIVE BROWNIAN POLYMERS

For active Brownian particles (ABPs), the orientation e^i of the self-propulsion force is different from that of tangentially driven active polymers (TDAPs), and it is given by

$$\dot{e}^i(t) = \boldsymbol{\eta}^i(t) \times e^i(t), \quad (\text{S1})$$

where $\boldsymbol{\eta}$ is a Gaussian white noise that has $\langle \boldsymbol{\eta}^i(t) \rangle = 0$ and $\langle \boldsymbol{\eta}^i(t) \cdot \boldsymbol{\eta}^j(t') \rangle = 2k_B T \gamma_r^{-1} \delta^{ij} \delta(t - t')$, with γ_r as the rotational friction coefficient. We set the rotational friction coefficient for ABPs as $\gamma_r = \gamma_t \sigma^2 / 3$.

Figure S1 shows that with increasing the number of monomers m , active Brownian polymers (ABPOs) accumulate in high-activity regions, which is further enhanced

by increasing m . However, as discussed in the main paper, TDAPs accumulate in low-activity regions, which is enhanced with increasing m .

Figure S2 shows the effect of the bulk density of monomers ρ_0 on ABPO and TDAP accumulation. Each polymer has 20 monomers and the activity field is given by $f_a = 10(1 - |z|/30)$. Increasing the bulk density of ABPOs significantly reduces their accumulation in

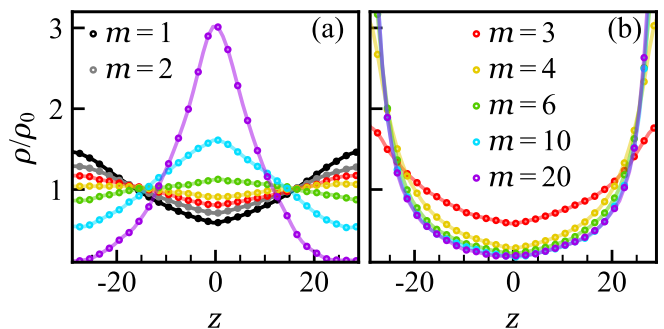


FIG. S1. Steady state density of (a) ABPO and (b) TDAP monomers along the z axis. Polymers have m monomers and $\rho_0 = 0.002$. The activity field is given by $f_a = 10(1 - |z|/30)$.

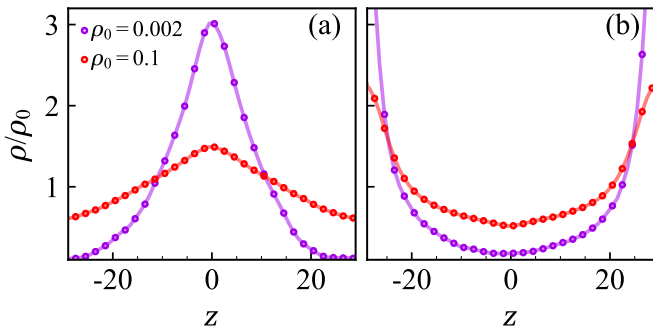


FIG. S2. Steady state density of (a) ABPO and (b) TDAP monomers along the z axis for varying bulk densities ρ_0 . Polymers have 20 monomers, and the activity field is given by $f_a = 10(1 - |z|/30)$.

high-activity regions, while TDAP accumulation in low-activity regions slightly decreases because of saturation.

EFFECT OF TDAP'S HEAD MONOMER ACTIVITY

We change the activity of the head monomer of a TDAP. Figure S3 presents the results for TDAPs connected to a passive monomer, an ABP, or a tangent monomer. There is no significant difference between the case where the head is passive or tangent. However, the accumulation in low-activity regions is slightly enhanced when the head monomer is an ABP.

EFFECT OF POLYMER CONFORMATION

In Fig. S4, we vary the equilibrium angle θ_0 from 60° to 180° . As θ_0 increases from 60° to 120° , the accumulation of ABPOs increases in high-activity regions, and

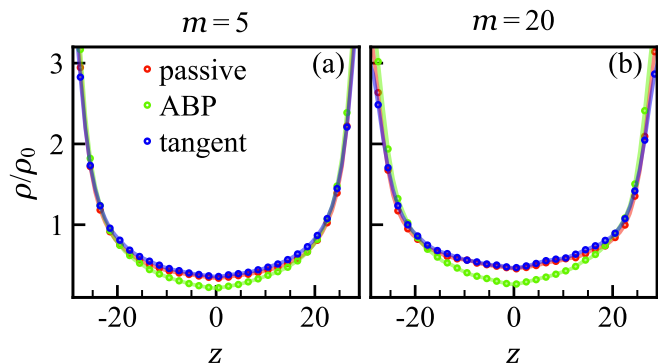


FIG. S3. Steady state density of TDAP monomers along the z axis for (a) $m = 5$ and (b) $m = 20$. The head monomer is either passive, an ABP, or tangent (along the bond). The bulk density $\rho_0 = 0.002$, and the activity field is given by $f_a = 10(1 - |z|/30)$.

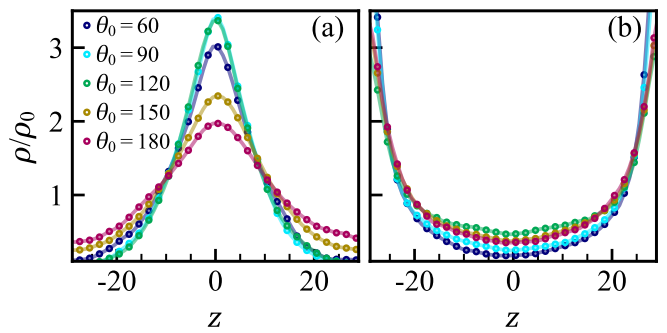


FIG. S4. Steady state density of monomers with $m = 20$ along the z axis for (a) ABPOs and (b) TDAPs for varying θ_0 (see Eq. (3) of the main manuscript). The bulk density $\rho_0 = 0.002$, and the activity field is given by $f_a = 10(1 - |z|/30)$.

the accumulation of TDAP in the low-activity region is suppressed. For $\theta_0 > 120^\circ$, the polymer adopts an increasingly rod-like conformation, leading to a significant reduction in ABPO accumulation in high-activity regions and an increase in TDAP in low-activity regions, as the steric constraints and propulsion alignment become more pronounced.

EFFECT OF ARM CHARACTERISTICS ON ACCUMULATION

In Fig. 2(b) of the main manuscript, we show that two-arm polymer accumulation varies with arm length, where the normalized steady-state density of all monomers is calculated. Figure S5 presents the steady-state density of the polymer core. The minimum accumulation of core in the high-activity region is observed for $m = 2$, and at $m > 2$, the accumulation in the high-activity region is enhanced. Increasing m further does not significantly affect accumulation.

Moreover, in Fig. 2 of the main manuscript, we show that two-arm TDAPs accumulate in high-activity regions

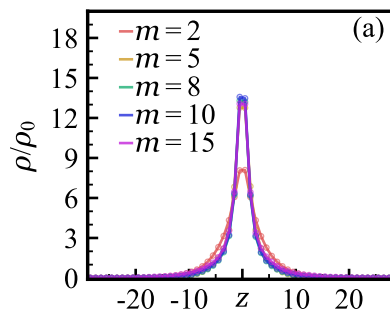


FIG. S5. Steady state density of the center of mass of two-arm polymers along the z . Arms are outward-directed and symmetric, each with m monomers. The bulk density $\rho_0 = 0.002$, and the activity field is given by $f_a = 10(1 - |z|/30)$.

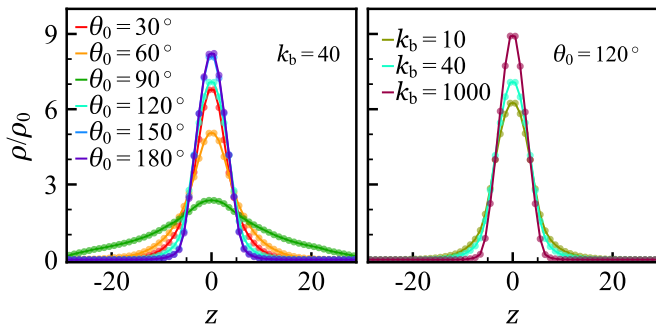


FIG. S6. Steady-state density distribution of monomers of starlike TDAPs along the z axis for varying (a) θ_0 and (b) k_b . Polymers have two symmetric arms, each containing $m = 5$ monomers. The self-propulsion force on each monomer of arms is toward the tip and tangent to the arm. The activity field is given by $f_a = 10(1 - |z|/30)$, and the bulk monomer density is set to $\rho_0 = 0.002$.

when the arms are propelled outward from the core to the tip and accumulate in low-activity regions when propelled inward from the tip to the core. To investigate the effects of conformation and rigidity on accumulation, we vary θ_0 and k_b . As θ_0 and k_b increase, the polymer becomes more stretched and rigid, respectively, leading to enhanced accumulation in high-activity regions (see Fig. S6). This effect arises because the tug-of-war between the arms intensifies, increasing the net propulsion toward higher activity regions.

Figure S7(a) presents the results for polymers consisting of a passive core and two asymmetric TDAP arms. The total number of active monomers is fixed at 20, and we vary the fraction x , defined as the length ratio between the shorter and longer arms (see schematic in Fig. S7(a)). The polymer exhibits strong accumulation in high-activity regions when the arms are symmetric ($x = 0.5$). However, as the arms become increasingly asymmetric (decreasing x), the polymers gradually migrate to low-activity regions and accumulate in low-

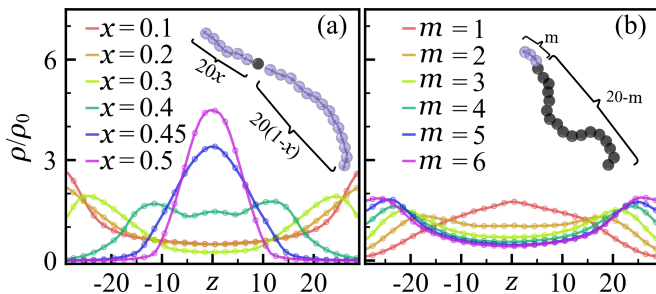


FIG. S7. Steady state density of monomers along the z . (a) Arms are outward-directed and asymmetric, with one having $20x$ and the other one $20(1-x)$ monomers. (b) A pulling TDAP with m monomer connected to a passive polymer with $20 - m$ monomers. The bulk density $\rho_0 = 0.002$, and the activity field is given by $f_a = 10(1 - |z|/30)$.

activity regions. This accumulation response becomes prominent in extreme asymmetry ($x < 0.2$). Interestingly, at intermediate asymmetry ($x \approx 0.4$), the polymer density profile exhibits a distinctly bimodal shape, indicating coexistence or competition between arms to migrate toward low- and high-activity regions. This transition suggests a delicate balance between pulling toward these regions, which arises from the asymmetric propulsion of the two arms, causing the polymer to fluctuate between these two regions.

In Fig. S7(b), the polymer consists of a passive segment pulled by an active TDAP. The polymer has a fixed total length of 20 monomers, and we vary the number of active monomers (m) at one end. For $m = 1$, the polymers accumulate modestly in high-activity regions. As m increases, we observe the formation of distinctly bimodal density profiles. This indicates that the polymer spends comparable amounts of time in both high- and low-activity regions, preferentially more time in the low-activity regions.

In Fig. S8, we present results for polymers of length m , where the first m^a monomers at the head are active and the rest are passive. When only a single monomer is active ($m^a = 1$), long polymers ($m \geq 15$) tend to accumulate in high-activity regions. However, as the number of active monomers increases, this accumulation decreases. For $m^a > 2$, the polymers accumulate in regions between the highest and lowest activity levels for the range of m studied here.

EFFECT OF ACTIVITY GRADIENT AND ASTER DENSITY ON ASTER ACCUMULATION

In Fig. 3(b) of the main manuscript, we show that polymers accumulate in the high-activity regions when the propulsion of TDAPs forming a multi-arm aster is outward from the core to the tips. Figure S9(a) presents the results for multi-arm polymers in an activity gradient given by $f_a = f_a^*(1 - |z|/30)$ for varying f_a^* . It shows that the accumulation of asters in the high activity region is robust and is not affected by f_a^* .

Additionally, as the number of asters in the simulation box increases, the accumulation in the high-activity regions decreases due to excluded volume effects. At higher densities, particles progressively saturate the highest activity regions, reducing the available space for further accumulation. Since these regions can only accommodate a limited number of asters without overlap, excess asters are displaced into adjacent lower-activity areas.

CONFINED TDAPs

We present the results for TDAPs connected to a passive and attractive particle in Fig. 5 of the main

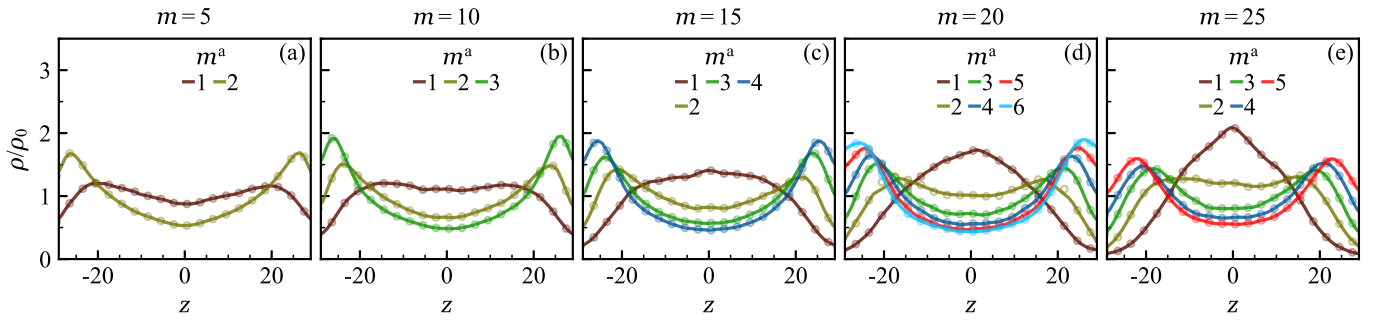


FIG. S8. Steady state density of monomers along the z . A pulling TDAP with m^a monomer connected to a passive polymer. The total number of polymer monomers is m . The bulk density $\rho_0 = 0.002$, and the activity field is given by $f_a = 10(1 - |z|/30)$.

manuscript. The interactions of active particles are described by Eq. (1) of the main manuscript. The passive-passive particle interactions are described by the Lennard-Jones (LJ) potential

$$U_{\text{LJ}}^{ij}(r) = \begin{cases} 4\epsilon \left[\left(\frac{\sigma^{ij}}{r^{ij}} \right)^{12} - \left(\frac{\sigma^{ij}}{r^{ij}} \right)^6 \right], & r^{ij} < 2.5\sigma^{ij}; \\ 0, & \text{otherwise;} \end{cases} \quad (\text{S2})$$

where r^{ij} is the distance between the particles i and j , ϵ the depth of the potential well, and $\sigma^{ij} = 0.5(\sigma^i + \sigma^j)$ is their interaction diameter.

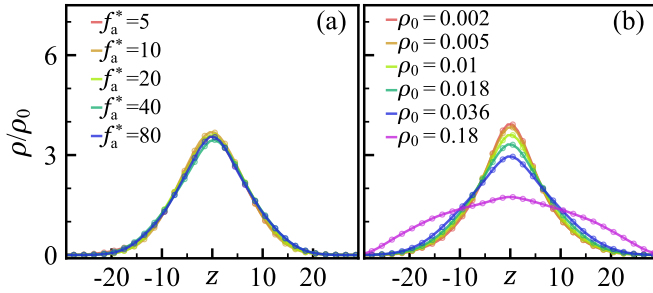


FIG. S9. (a) Steady-state density of monomers along the z . Each arm has $m = 10$ monomers, the bulk density is $\rho_0 = 0.002$, and the activity field is given by $f_a = f_a^*(1 - |z|/30)$ for varying f_a^* . (b) Steady-state density of monomers along the z for varying bulk density ρ_0 . Each arm has $m = 5$ monomers, and the activity field is given by $f_a = 10(1 - |z|/30)$.